Journal of Marine Research, 63, 1057–1083, 2005

Parameterizations of Lagrangian spin statistics and particle dispersion in the presence of coherent vortices

by Milena Veneziani[1,2], Annalisa Griffa[1,3], Andy M. Reynolds[4], Zulema D. Garraffo[1] and Eric P. Chassignet[1]

ABSTRACT

Coherent vortices are known to play an important role in transport processes of ideal flows such as two-dimensional and quasi-geostrophic turbulent flows. In this paper, their effect on eddy dispersion and diffusivity is studied in a realistic oceanic flow, using synthetic Lagrangian data simulated within a high-resolution ocean general circulation model in the Gulf Stream recirculation region. The possibility of using a Lagrangian Stochastic Model (LSM) with nonzero mean spin statistic, Ω, to parameterize the observed characteristics is considered. The probability distribution of the Ω parameter (which is representative of the looping behavior of trajectories embedded inside the coherent vortices) is also studied.

The main result is that the LSM with a tri-modal Ω-distribution is able to reproduce the eddy diffusivity and dispersion characteristics, especially at short and intermediate time scales. Particularly well predicted are the effects of the coherent vortices, which are the enhanced spreading of particles at short times due to the high eddy energy of the vortices and the inhibited diffusion at intermediate times due to the vortex trapping mechanisms. The LSM parameterization of eddy dispersion is shown to be more appropriate than the commonly used asymptotic eddy-diffusivity approximation. More complex than tri-modal distributions of mean spin are also considered in the LSM, and they are found to produce only slight changes in the predictions of eddy statistics and dispersion.

1. Introduction

The transport of passive tracers in the ocean depends on the interaction of a very broad spectrum of scales of motion. It is, therefore, very challenging to describe and predict a tracer evolution, and simplifying assumptions are necessary in order to study the problem either mathematically or computationally. For large-scale climate applications, it is usually assumed that the velocity field can be described as the sum of a large-scale mean (resolved) component, $\mathbf{U}$, and a mesoscale eddy (unresolved) component, $\mathbf{u}'$, and that a spectral gap between the two components exists. The tracer evolution is then governed by the mean

1. Rosenstiel School of Marine and Atmospheric Sciences, Meteorology and Physical Oceanography Division, University of Miami, Miami, Florida, 33149, U.S.A.
2. Corresponding author. ***email: cveneziani@rsmas.miami.edu***
3. IOF/CNR, La Spezia, Italy.
4. Rothamsted Research, Harpenden, United Kingdom, AL5 2JQ.

flow advection and the eddy field diffusion and mixing. The (unresolved) eddy effects have to be parameterized in terms of the resolved large scales so that a closed equation for the tracer evolution can be obtained.

The simplest and most commonly used parameterization model describes the diffusion effects of the eddy field as acting against the gradient of the mean tracer distribution, through a proportionality coefficient that is the eddy-diffusivity, K. Such an approximation is strictly valid only when the scales of the eddy field are infinitesimal compared with the scales of the mean flow (e.g., Tennekes and Lumley, 1972). The asymptotic, single-parameter, eddy-diffusivity theory is expected to hold for weakly energetic, quasi-homogeneous regions of the ocean. It may be too restrictive for regions characterized by strong and quickly varying mean flows in which the mesoscale eddy field contributes actively at scales comparable with those of the mean flow, and for regions dominated by highly energetic coherent structures such as mesoscale vortices and planetary waves which alter the diffusion properties of tracers.

Alternative parameterization models of eddy transport can be introduced in the Lagrangian framework. The nonasymptotic, multi-parameter, Lagrangian Stochastic Models (LSMs) describe the motion of passive tracer particles in a turbulent flow using stochastic differential equations. They have been used extensively in the prediction of dispersion and eddy statistics in atmospheric and oceanographic flows (e.g., Thomson, 1986; Griffa, 1996; Falco *et al.,* 2000; Berloff and McWilliams, 2002; Bauer *et al.,* 2002; Reynolds, 2002). LSMs can be classified in terms of the number of time scales that they incorporate. At the first-order, a finite time scale, the Lagrangian decorrelation scale T_L, is associated with the eddy velocity field and considered representative of the energy-containing scales of motion; at the second-order, another finite scale is introduced and associated with the acceleration field, etc. First- and higher-order LSMs are therefore suitable to describe the eddy field in the most energetic and dynamically complex regions of the ocean. Furthermore, since they are able to predict eddy diffusion properties at short, as well as long, time scales, LSMs can provide a more complete description of the eddy contribution in the presence of coherent structures than the asymptotic eddy-diffusivity parameterization.

In two recent papers, Veneziani *et al.* (2004, 2005, hereafter referred to as V04 and V05, respectively) have investigated the effects of coherent vortices on the eddy properties in the North Atlantic recirculation region and the applicability of a suitable LSM to the observed results. In V04, the analysis of *in-situ* floats at 700 m shows that, in agreement with previous findings by Richardson (1993) and Rupolo *et al.* (1996), Lagrangian statistics are characterized by the superposition of two different regimes associated with two distinct types of trajectories. Fast rotating floats, so-called "loopers," are trapped in Gulf Stream rings and lenses, and are mainly responsible for oscillating eddy statistics. Nonlooping floats are instead associated with the "disorganized," typically less energetic, background eddy field. The observed eddy characteristics in both regimes are found to be well reproduced by a first-order, two-dimensional LSM with a bi-modal distributed mean spin parameter Ω. The spin couples motions in the zonal and meridional direction thereby

endowing trajectories with a preferred sense of rotation. By associating finite values of Ω to the looping trajectories and zero values of Ω to the nonlooping floats (bi-modality hypothesis), the LSM is able to describe the effects of both the loopers and the nonloopers regimes. In V05, the Eulerian physical meaning of the spin parameter is investigated by using an extensive numerical trajectory data set simulated within the high-resolution (1/12°) Miami Isopycnic Coordinate Ocean Model (MICOM). Through the analysis of both the Lagrangian data and the MICOM-predicted Eulerian fields, it is shown that Ω is directly related to the Eulerian vorticity of the coherent vortices which are responsible for the looping floats behavior.

This progress leaves two main open questions. The first concerns the ability of the LSM to capture accurately the single-particle dispersion function $D(t)$, defined as the mean squared eddy displacement $\langle x'^2 \rangle$ (where $\langle\ \rangle$ denotes an ensemble average process), and the eddy diffusivity $K^*(t)$, defined as the dispersion rate of change $\frac{1}{2}\mathrm{d}D/\mathrm{d}t$. In V04, the model performance was tested mostly in terms of velocity autocovariance and crosscovariance functions because the limited availability of *in-situ* data did not allow for a complete description of the dispersion and diffusivity characteristics, especially at asymptotic time scales. These eddy statistics are, however, of primary importance in studies of tracer evolution and should be tested to validate a suitable parameterization model. The second question concerns the actual shape of the probability distribution (pdf) of the mean spin Ω. Although the Ω-pdf was previously assumed to be bi-modal (or tri-modal, when both cyclonic and anticyclonic loopers were present), estimates of Ω values from single trajectories carried out in V04 and V05 suggested that a more complex spin distribution could exist in some regions of the northwestern Atlantic.

These two open questions provide motivation for the present paper. They are addressed by considering the same data set analyzed in V05, which consists of the MICOM numerical Lagrangian trajectories homogeneously released at 700 m depth over a $1° \times 1°$ spatial grid. The synthetic floats are redeployed every month during an overall MICOM simulation period of one year. Such an extensive data set facilitates the robust prediction of dispersion characteristics and spin distribution. The investigation is carried out in the southern Gulf Stream recirculation region, referred to as RINGS in V05, which is a region characterized by an abundance of mesoscale coherent vortices (the MICOM Lagrangian data and the dynamical characteristics of RINGS are thoroughly described in V05). In the first part of the paper, the dispersion, D, and the diffusivity function, K^*, are evaluated from the MICOM floats and the role played by coherent vortices in characterizing the statistics is isolated and discussed. The results are then compared to those predicted by the LS model with spin and to the results obtained by simply applying the asymptotic eddy-diffusivity approximation. In the second part of the paper, the distribution of the mean spin parameter is investigated by computing Ω frequency histograms from the MICOM trajectory data in RINGS. The results are also used to suggest and test different Ω-pdfs to be utilized in the LSM.

The paper outline is as follows. Section 2 provides a brief overview of the LSM, while

Table 1. Eddy parameters used in the Lagrangian stochastic model simulations, for the nonlooping (no-loop), the cyclonic (cycl), and the anticyclonic (acycl) trajectories. The parameters are the velocity variance, σ^2, the decorrelation time scale, T_L, and the mean spin, Ω. Also shown is the percentage of each simulated trajectory subset, which is taken directly from MICOM float statistics (see V05 for details).

	σ^2 (cm^2 s^{-2})	T_L (days)	Ω_0 (days^{-1})	%
no-loop	50	12	0.00	73.8
cycl	130	15	0.25	21.0
acycl	70	15	−0.15	5.2

Sections 3 and 4 are devoted to testing parameterizations of the eddy statistics. The investigation of the spin distribution is included in Section 5. Summary and main conclusions are finally presented in Section 6.

2. The Lagrangian stochastic model

The Lagrangian stochastic model that will be used as a main benchmark for the parameterization tests is a first-order, two-dimensional model with nonzero mean spin statistics [for a general discussion on this type of LSMs the reader is referred to Borgas *et al.* (1997), Sawford (1999), and Reynolds (2003)].

The model describes the evolution of the eddy velocity field along Lagrangian trajectories through the following equations,

$$\begin{aligned} \mathrm{d}u' &= -u' T_{Lu}^{-1}\mathrm{d}t - \Omega v'\mathrm{d}t + (2\sigma_u^2/T_{Lu})^{1/2}\mathrm{d}\xi_u, \\ \mathrm{d}v' &= -v' T_{Lv}^{-1}\mathrm{d}t + \Omega u'\mathrm{d}t + (2\sigma_v^2/T_{Lv})^{1/2}\mathrm{d}\xi_v, \end{aligned} \tag{1}$$

where σ^2 is the velocity variance given by $\langle u'^2 \rangle$ (subscripts u, v stand for either zonal or meridional components) and the mean spin Ω is equal to $\langle u'\mathrm{d}v' - v'\mathrm{d}u' \rangle / 2\Delta t$ EKE (Sawford, 1999), in which the eddy kinetic energy EKE is given by $0.5(\sigma_u^2 + \sigma_v^2)$. The random increment $\mathrm{d}\xi$ is a Wiener process with independent components, zero mean, and variance equal to the sampling interval Δt.

In the LSM applications of this paper, the parameters in (1) are estimated from the ensemble of MICOM trajectories longer than 15 days present in the RINGS region. Results obtained from the separated subsets of the nonloopers, the cyclonic, and the anticyclonic trajectories are listed in Table 1. The estimation of T_L and Ω is performed as in V04 and V05, i.e., the Lagrangian decorrelation time scale is computed from the autocovariance statistics assuming that the autocovariances are described by (1), and the mean spin is calculated from the crosscovariance functions. The separation of loopers and nonloopers is carried out by applying the Ω-threshold criterion introduced in V04 and V05; that is, after estimating the mean spin from each single float, a trajectory is considered as a looper if its $|\Omega|$ value is higher than 0.1 days^{-1}.

The benchmark LSM simulation considered in Section 3 is carried out by assuming a

tri-modal distribution of Ω, similar to what was performed in V04 (generalizations to more complex distributions are considered in Section 5). The three fixed values of mean spin Ω_0 listed in Table 1 are, therefore, used to simulate nonlooping, cyclonic, and anticyclonic trajectories. The probability associated with each family of LSM trajectories is dictated by the actual distribution of MICOM floats, given by the percentage of loopers and nonloopers in Table 1. In order to reproduce the situation of the MICOM floats in RINGS, the LSM particles are launched inside a box 2000 km long and 300 km wide, and only trajectories falling inside this region are taken into account to evaluate the statistics.

3. Eddy statistics, dispersion, and LSM parameterization

The goal of this section is to investigate the main eddy statistics of the MICOM floats and to assess whether model (1) is able to describe and parameterize both the diffusion and dispersion characteristics of the background eddy field and the anomalous diffusion properties produced by strong coherent vortices. In Section 4, the results will then be compared to those obtained by applying the commonly used eddy-diffusivity parameterization method.

As a first step, we consider the eddy velocity autocovariance and crosscovariance functions, which, in homogeneous and stationary turbulence, are defined as $R_{uu}(\tau) = \langle u'(t)u'(t+\tau)\rangle$ and $R_{uv}(\tau) = \langle u'(t)v'(t+\tau)\rangle$, respectively (similar notations apply for the other statistical components). The eddy field $\mathbf{u}'$ is computed by subtracting the mean flow $\mathbf{U}$ from the total Lagrangian velocities. The mean flow is in turn obtained by averaging the MICOM Eulerian velocities spatially over $1^\circ \times 1^\circ$ bins and temporally over the one-year period during which the trajectories were simulated (different mean flow estimates were also considered and they are discussed in the Appendix of V05). The statistics obtained from the MICOM floats and from the LSM-simulated trajectories are presented in Figure 1 for the autocovariances, and in Figure 2 for the crosscovariance statistics. Also drawn is the 95% Confidence Limit (C.L.) estimated as $2\sigma^2/(n^*)^{1/2}$ for the autocovariances (Priestley, 1981), and as $2[(\sigma_u^2\sigma_v^2 - \sigma_{uv}^2)/n^*]^{1/2}$ for the crosscovariances (Sciremammano, 1979), where $\sigma_{uv} = \langle u'v'\rangle$ and n^* is the number of independent data at each time lag. This is equal to $n\Delta t/2T_L$, where n is the total number of data and T_L is taken as 10 days (V04; Owens, 1991). The statistics are computed from the overall trajectory ensemble (Figs. 1–2a, d), and separately from the nonloopers (Figs. 1–2b, e) and the cyclonic trajectory subsets (Figs. 1–2c, f; results from the anticyclonic loopers are not shown because of the low percentage of anticyclones present in RINGS).

The MICOM overall zonal autocovariance exhibits a first positive lobe at $t \approx 20$ days that is more pronounced than the first negative lobe. As discussed in V05, this is due to the superposition of the oscillating loopers statistics with the exponentially decaying nonloopers autocovariances. Another characteristic that is particularly evident for the nonloopers subset (Fig. 1b) is the anisotropic behavior of the statistics, with the meridional autocovariance function exhibiting lower values than the zonal autocovariance and a tendency toward developing a negative tail. Two possible mechanisms can be considered responsible for the

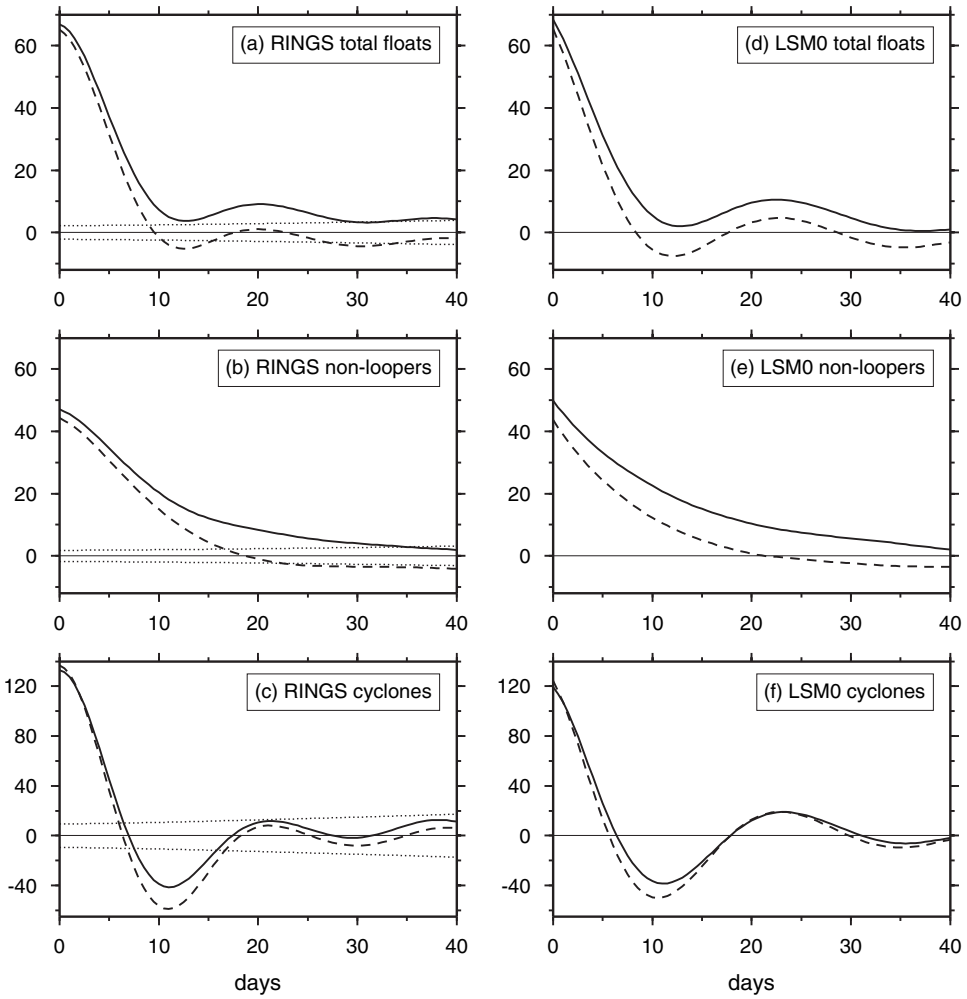

Figure 1. Lagrangian velocity autocovariance functions ($cm^2\ s^{-2}$) from MICOM floats in region RINGS (left panels) and from LSM trajectories (right panels). Results are obtained from the overall Lagrangian data (a, d), and separately from the nonloopers (b, e) and the cyclonic trajectories (c, f). Solid (dashed) lines indicate zonal (meridional) autocovariances, while the dotted lines denote the 95% C.L., computed as $2\sigma^2/(n^*)^{1/2}$.

statistical anisotropy. First, the anisotropy can be related to the data sampling in RINGS and to the fact that the region is far more extended in the zonal than in the meridional direction. In such a configuration, fast moving meridional floats tend to exit the region relatively quickly, so that the statistics at later times are influenced by slowly moving meridional particles and by longer-lived zonal floats. Second, the anisotropy can be produced by real physical processes, which tend to inhibit meridional dispersion while

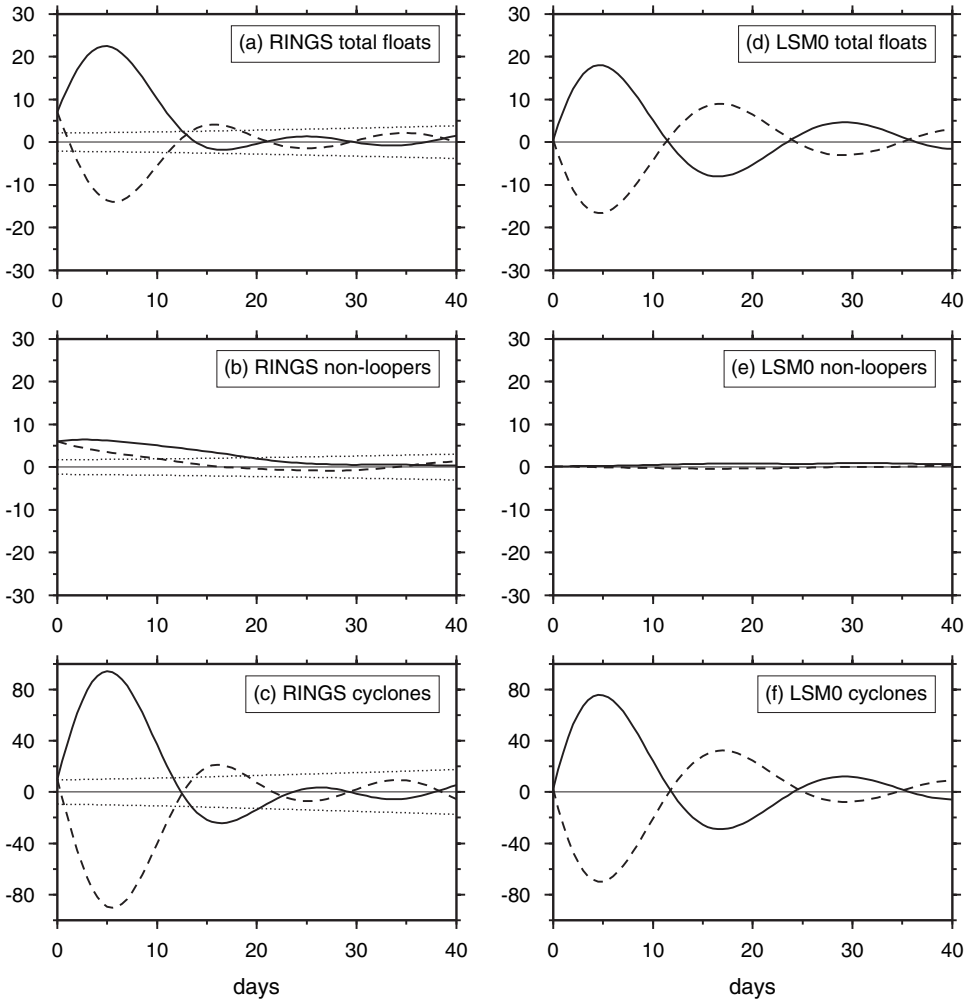

Figure 2. Similar to Figure 1, but for the velocity crosscovariance functions. The 95% C.L. is computed as $2[(\sigma_u^2\sigma_v^2 - \sigma_{uv}^2)/n^*]^{1/2}$.

enhancing zonal spreading of particles. Possible physical mechanisms include conservation of potential vorticity (O'Dwyer *et al.,* 2000; LaCasce and Speer, 1999) and spatial inhomogeneities. These two aspects are investigated in detail in the Appendix, and both are found to influence the observed anisotropy. The two effects, however, cannot be separated because of the inhomogeneity and the dynamically complex features of the area. It is, in fact, difficult to identify a region of interest that is at the same time homogeneous, equally extended in the meridional and zonal directions, and sufficiently broad to provide enough data for significant statistics. Consequently, the results as a whole have to be considered as representative of the specific region under examination.

When considering the statistics computed from the LSM-simulated trajectories (Figs. 1–2d,e,f), we see that the first-order LSM with the tri-modal distributed Ω is quite successful in reproducing the MICOM eddy characteristics, as was found to be the case for *in-situ* data in V04. Regarding the anisotropic behavior of the LSM statistics, we notice that the anisotropy is not incorporated into the LS model (the parameters in Table 1 are isotropic, for reasons that will be better explained in the Appendix) but is due to the effect of having considered only LSM-trajectories that fall inside a rectangular box resembling the shape of the RINGS region. This supports the argument that the statistical anisotropy observed in the MICOM floats is partly due to the elongated shape of RINGS (see the Appendix).

As a next step, we consider eddy statistics that give a more direct assessment of the particle dispersion due to the turbulent flow contribution. The Lagrangian eddy diffusivity K^* can be easily related, for stationary and homogeneous flows, to the velocity autocovariance function, R (reference to the velocity components is suppressed for simplicity of notation), through the Taylor's theorem (Taylor, 1921),

$$K^*(t) = \int_0^t R(\tau)\mathrm{d}\tau. \tag{2}$$

By applying this relationship, K^* has been determined for the overall Lagrangian data, the nonloopers, and the loopers subsets. The results are shown in Figure 3 for the MICOM floats (a–c panels) and for the LSM-simulated trajectories (d–e panels). Although the diffusivity results are linked to those for the autocovariance function, their inspection is instructive because they provide a more direct description of the dispersion properties, especially at long and asymptotic times.

The MICOM nonlooping trajectories give rise to diffusivities that increase approximately monotonically up to their asymptotic value (Fig. 3b), while the looping floats produce diffusivity functions that oscillate substantially before reaching their saturation level (Fig. 3c). Furthermore, at times shorter than 10 days, the diffusivity of the loopers is much larger than that of the nonloopers, while the situation is reversed at times longer than 15 days. An approximately constant saturation level is reached for both loopers and nonloopers at $t \gtrsim 40$ days.

These results are in general agreement with the Taylor theory (Taylor, 1921). For $t \ll T_L$, during the so-called ballistic regime, $R \to \sigma^2$ and $K^*(t) \to \sigma^2 t$, so that the tracer diffusivity is directly proportional to the intensity of the eddy field. The spreading rate of loopers is therefore initially greater than the spreading rate of the less energetic nonloopers. At later times, the random walk diffusive regime is reached and

$$K^*(t) = K = \sigma^2 T_i, \tag{3}$$

where T_i is the integral time scale equal to $\sigma^{-2}\int_0^\infty R(\tau)\mathrm{d}\tau$. The diffusivity of the loopers is less than that of the nonloopers because the suppression in diffusivity due to the effects of a

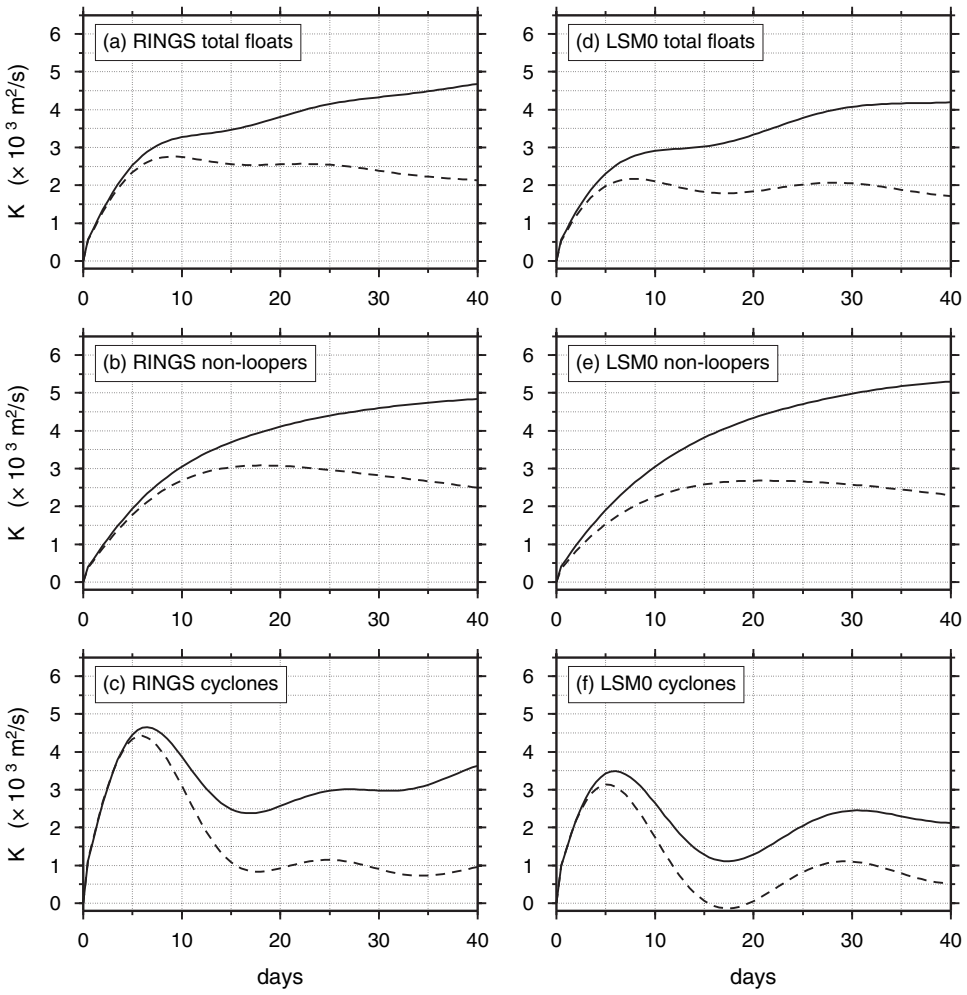

Figure 3. Similar to Figure 1, but for the Lagrangian eddy diffusivity function K^*.

nonzero mean spin are greater than the enhancement in diffusivity associated with higher eddy kinetic energies.

As for the autocovariances, the eddy diffusivity functions obtained from the MICOM floats are qualitatively well described by the corresponding statistics estimated from the Lagrangian stochastic model trajectories (Fig. 3d, e, f), especially for the overall data and at short and intermediate time scales. The tri-modal LSM is therefore able to represent well both the diffusion properties of the background eddy field and the intermediate-time subdiffusive processes induced by the energetic mesoscale coherent vortices.

Such findings are confirmed and strengthened when considering the eddy dispersion function D, estimated as $\langle x'^2 \rangle$, where x' is determined by integrating the Lagrangian

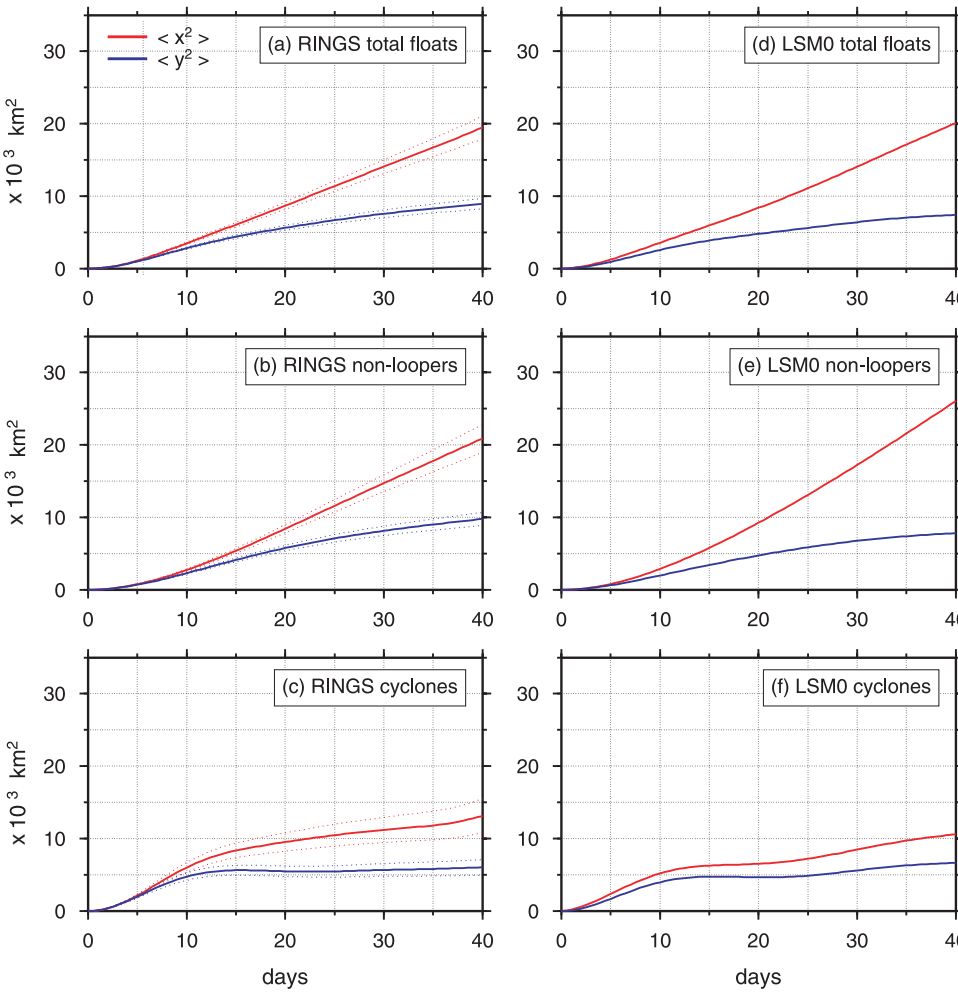

Figure 4. Similar to Figure 1, but for the eddy dispersion function D. Red (blue) lines denote zonal (meridional) dispersion, while the 95% C.L. is computed for each component as $1.96D[2/(n^* - 1)]^{1/2}$.

velocity u' along each trajectory with respect to an arbitrary initial position, x_0, common to all floats (Berloff *et al.,* 2002). The ensemble average $\langle\ \rangle$ is again carried out for the overall Lagrangian data, the loopers, and the nonloopers subsets. The results are presented in Figure 4, with the zonal (meridional) dispersion shown as a red (blue) solid line. The 95% C.L., estimated as $1.96D[2/(n^* - 1)]^{1/2}$ (LaCasce, 2000), is also drawn (the error has to be considered as a lower estimate of the real error because it does not take into account uncertainties related to the u' integration process).

Similar to the results obtained from the diffusivity functions, at times shorter than 10–15

days, the MICOM loopers exhibit higher dispersion values than those shown by the nonloopers (Fig. 4b, c). On the other hand, at times longer than 15 days the nonloopers dispersion reaches values up to twice as much as those exhibited by the loopers statistics. These characteristics are once again well reproduced by the LSM for the loopers and nonloopers subsets and for the overall data (Fig. 4d, e, f).

4. Eddy-diffusivity parameterization

The eddy-diffusivity is the simplest parameterization for the eddy spreading of passive tracers. It is valid at asymptotically long times and is, therefore, equivalent to a zeroth-order LSM (e.g., Csanady, 1980). Despite its simplicity, the eddy-diffusivity model is commonly used in Ocean General Circulation Models (OGCMs). For this reason, it is useful to explicitly test its performance in the presence of coherent structures. Furthermore, an important question in eddy-diffusivity applications is how to determine the parameter K from the data, and how sensitive the results are to the estimation method. These points will be addressed in the following using the MICOM data.

In principle, the most natural way to estimate K is to use Lagrangian data and evaluate the asymptotic value of $K^*(t)$ from (2),

$$K = \lim_{t\to\infty} K^*(t) = \int_0^\infty R(\tau)\mathrm{d}\tau.$$

The difficulty of this estimation lies in its asymptotic nature. Even in ideal homogeneous regions, long temporal records and extensive sampling are necessary to provide statistically significant estimates of eddy diffusivity at the saturation regime. Indeed, in many real oceanic applications, flow inhomogeneities may affect the concept of asymptotic regime.

In practical applications involving observed or numerical trajectories, the asymptotic regime is often assumed to be reached and the integration is stopped at finite times (e.g., Boning and Cox, 1988; Figueroa and Olson, 1994; Bauer *et al.,* 1998, 2002; Falco *et al.,* 2000). Alternatively, K is determined from expression (3), with the integral time scale T_i estimated by simply integrating the velocity autocovariance function R up to the first zero crossing (e.g., Freeland *et al.,* 1975; Krauss and Boning, 1987; Figueroa and Olson, 1994; Poulain and Niiler, 1989; Lumpkin and Flament, 2001; Lumpkin *et al.,* 2002). This method is expected to give reasonable results when R is exponentially decorrelating in time, but is expected to overestimate T_i (and K) when the autocovariance exhibits strong oscillations at intermediate times. Finally, K can be computed using theoretical expressions of eddy diffusivity predicted by suitable Lagrangian stochastic models (Griffa *et al.,* 1995; Griffa, 1996; Berloff and McWilliams, 2002). Once a particular LSM is assumed to apply, it can be used in a "inverse" manner to provide the theoretical K from (3) without having to rely on the estimate of asymptotic parameters.

When Lagrangian data are not available, K has to be estimated using Eulerian data. Satellite altimeter data, for example, were used by Stammer (1997, 1998) to compute the

eddy diffusivity either through a "mixing length," L_E, as $K \propto \sqrt{\text{EKE}}\, L_E$, or through an Eulerian decorrelation time scale, T_E, as $K \propto \text{EKE}\, T_E$. The eddy kinetic energy EKE was directly determined by using the altimeter data and assuming geostrophic approximation. The scales L_E and T_E were either computed from Eulerian autocorrelation functions (Stammer, 1997) or associated to eddy scales set by baroclinic instabilities and therefore estimated through climatological vertical density distributions (Held and Larichev, 1996; Stammer, 1998).

We first consider the Lagrangian estimate for K directly derived from (2), and we evaluate it from the MICOM data. From Figure 3, an approximate plateau can be seen for time scales between 20 and 40 days, providing $(K_x, K_y) \simeq (4.5, 2.5) \times 10^3\ \text{m}^2\ \text{s}^{-1}$ for the overall trajectory data, $(5.0, 2.8) \times 10^3\ \text{m}^2\ \text{s}^{-1}$ for the nonlooping floats, and $(3.0, 1.0) \times 10^3\ \text{m}^2\ \text{s}^{-1}$ for the looping trajectories. The predicted eddy dispersion functions D, calculated according to the Taylor theory as $2Kt$, are shown in Figure 5 for the various data sets. When comparing these results with the eddy dispersion computed directly from the MICOM floats (Fig. 4a, b, c), it is clear that the eddy-diffusivity parameterization tends to overestimate the actual particle dispersion in all cases, except for the loopers dispersion at short times which is underestimated. The overestimate is particularly high at times shorter than 20 days, during which it becomes up to 200% of the actual dispersion (the largest discrepancies are found in the zonal direction). At longer times this difference decreases, becoming approximately 50% of the MICOM floats dispersion at $t = 40$ days. This result is not surprising because the dispersion predicted by the eddy-diffusivity is fundamentally valid only at asymptotic times. The dispersion reproduced by the Lagrangian stochastic model simulation (Fig. 4d, e, f), on the other hand, describes the MICOM floats dispersion more accurately, especially at short and intermediate times.

We need to point out that, although some uncertainties are always associated with estimating a saturation level for K, the present results are obtained in "optimal" conditions, i.e., they are computed from an extended data set allowing for a meaningful estimation of the asymptotic diffusivity. For this reason, the suppressed levels of diffusion due to the effects of coherent vortices at long times have been partially taken into account. Results would be far worse if an "incomplete" integral time scale were calculated (as done for instance when integrating the correlation function up to the first zero crossing), because the predicted eddy diffusivity value would be affected by the high eddy energy associated with the coherent vortices, without being counterbalanced by the correct, very low value of integral time scale T_i.

The asymptotic estimates of K are now compared with those obtained through the "inverse" application of the LS model (1), which predicts a specific theoretical $K = \sigma^2 T_i$. While σ^2 is directly computed from zero-lag statistics, the integral time scale is obtained as a combination of nonasymptotic parameters by integrating the LSM theoretical autocovariance function. Specifically, for the nonloopers regime, a first-order LSM with zero value of mean spin can be hypothesized and the theoretical autocovariance takes the simple form $\sigma^2 e^{-\tau/T_L}$, so that $T_i \equiv T_L$. For the loopers regime, on the other hand, a finite value of Ω has

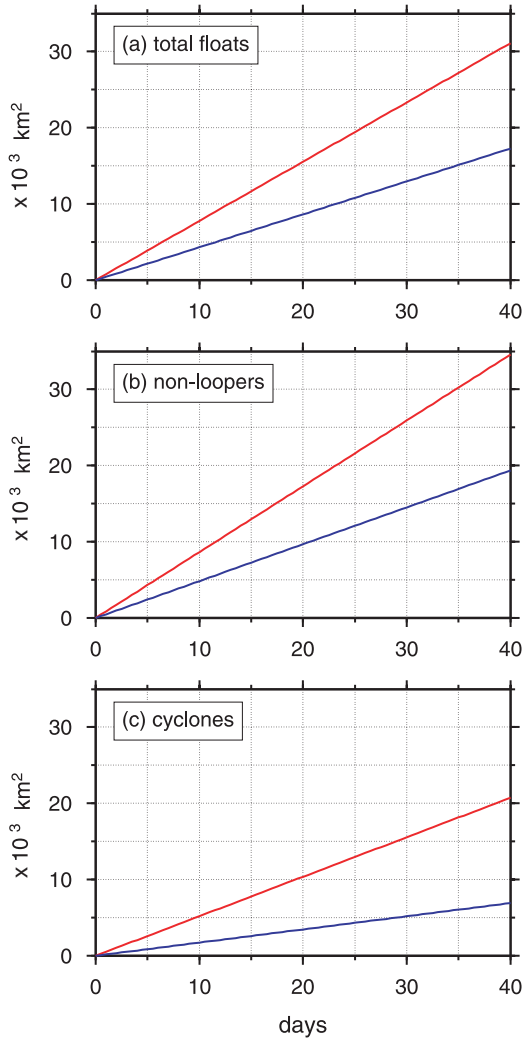

Figure 5. Eddy dispersion functions predicted through the asymptotic eddy-diffusivity approximation, using a Lagrangian saturation level K estimated from Figure 3. Results are for (a) the whole Lagrangian data set available in RINGS, (b) the nonloopers, and (c) the loopers subset.

to be considered and the LSM-predicted autocovariance becomes $\sigma^2 e^{-\tau/T_L} \cos(\Omega\tau)$, so that $T_i = T_L/(1 + T_L^2\Omega^2)$. The parameters σ^2, T_L, and Ω listed in Table 1 can therefore be used to compute two different values of asymptotic eddy diffusivity, K_{nl} and K_l, for the nonloopers and the loopers regimes, respectively. The results are K_{nl} (K_l) ≈ 5.2 (1.5) $\times$ 10^3 m^2 s^{-1}. The overall diffusivity can then be approximated by the weighted average $K = nK_{nl} + lK_l$, where n, l are the percentages of nonlooping and looping trajectories (divided by 100). From Table 1, approximately 75 (25)% of trajectories are nonloopers

(loopers), and the overall diffusivity is therefore given by $K = 4.3 \times 10^3$ m^2 s^{-1}. These K values are very close to the average asymptotic eddy diffusivities estimated above directly from the MICOM Lagrangian data, thus suggesting that the methodology could be successfully used to provide good estimates of K for low-resolution OGCMs.

As a final step, we now consider estimates of eddy diffusivity using Eulerian quantities and scaling arguments. We adopt the method suggested by Lumpkin *et al.* (2002), who found that in the Gulf Stream region between the surface and 700 m, it is more appropriate to compute the Eulerian diffusivity by means of a mixing length $L_E \approx 100$ km instead of using an Eulerian decorrelation time scale T_E. The authors showed that in the upper water column, the Lagrangian and Eulerian length scales are comparable, while the Lagrangian time scale is typically shorter than its Eulerian counterpart. We therefore estimate a $K \sim \sigma \cdot 100$ km, where σ is the velocity variance for each Lagrangian data set (overall, nonloopers, and loopers). This approximation yields $(K_x, K_y) = (8.2, 8.1) \times 10^3$ m^2 s^{-1} for the overall trajectory data, $(6.8, 6.6) \times 10^3$ m^2 s^{-1} for the nonloopers, and $(11.5, 11.7) \times 10^3$ m^2 s^{-1} for the loopers, which are values 2–3 times as large as the asymptotic diffusivities estimated from Lagrangian data. These results obviously overestimate overall eddy dispersion, mainly due to the excessive weight given to the high energy associated with the looping trajectories. It is equally evident, however, that such estimates of diffusivities are highly dependent upon the exact choice of mixing length L_E. An uncertainty of ± 50 km over L_E, due for example to horizontal or vertical flow inhomogeneities, would change dramatically the outcome value of K. For this reason, a more precise knowledge of Eulerian eddy scales distribution is necessary in order to have more appropriate Eulerian estimates of eddy diffusivity.

5. Spin probability distribution

In this section we explore the nature of the mean spin probability distribution and its parameterization in the Lagrangian stochastic model (1). Results from both *in-situ* floats and MICOM Lagrangian data reported in V04 and V05 suggest that the distribution of Ω may be more complex than the simple bi-modal (or tri-modal) distribution considered so far, which associates single finite values of mean spin to the loopers and a zero value of mean spin to the nonloopers.

In order to investigate this issue, we first computed the frequency histogram of the Ω parameter estimated by running averaging over 60-day periods along the MICOM trajectories in RINGS. The results are shown in Figure 6 for the overall Lagrangian data set (Fig. 6a), the nonlooping (Fig. 6b), and the looping trajectories (Fig. 6c), where the distinction between loopers and nonloopers was performed by evaluating an average spin value for each trajectory and by applying the Ω-threshold criterion.

The Ω-histogram for the overall floats shows that the highest probabilities ($\approx$74%) occur when Ω is in the range between -0.1 and 0.1 days^{-1}, which corresponds to what we have called the regime of the nonloopers. The remaining mean spin values are likely to be found between 0.1 and 0.35 days^{-1}, with a much smaller percentage of Ω values ($\approx$6%)

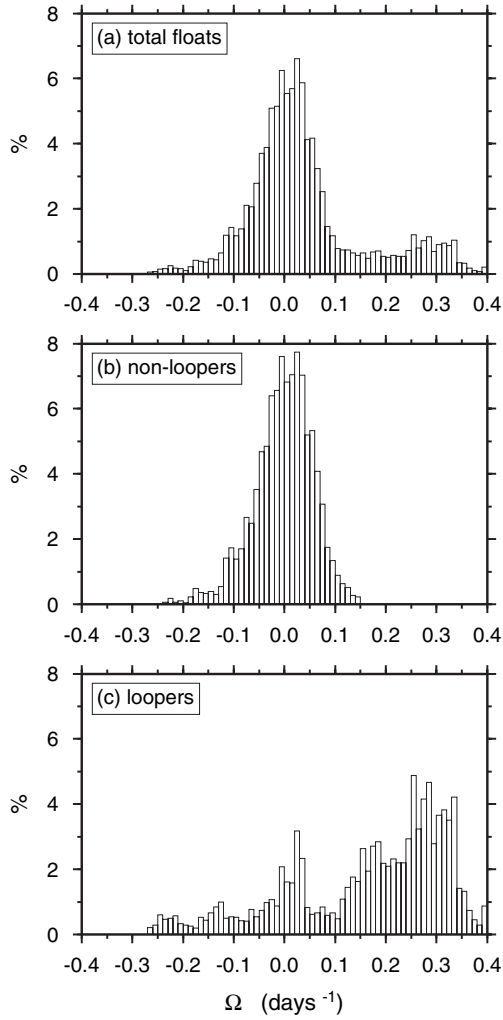

Figure 6. Frequency histogram of the 60-day running-averaged spin parameter obtained from the different data sets.

found in the negative range between -0.3 and -0.1 days^{-1}. This distribution is in good agreement with previous findings on nonloopers, cyclonic, and anticyclonic trajectory distribution [see Table 1, V04, and Richardson (1993)].

Although the results are certainly influenced by the finite data sampling, they clearly suggest that the Ω-pdf is more complex than bi-modal. In particular, positive (cyclonic) Ω values exhibit a rather flat distribution, with higher probabilities concentrated in the range 0.25–0.35 days^{-1}. This pattern could either be due to the presence of coherent vortices characterized by different time scales and consequently by different rotational dynamics,

or to the time variations of the Ω parameter associated with the evolution of the coherent vortices in which the loopers are embedded. The spin distribution could also be influenced by transitions between loopers and nonloopers, as discussed in V04 and V05. This phenomenon is suggested by the pattern of Ω-frequency histogram obtained from the separate nonloopers (Fig. 6b) and loopers subsets (Fig. 6c). In fact, although the majority of Ω values for the nonloopers (loopers) remain in the range $|\Omega| <(>) 0.1$, a number of mean spin values obtained from the nonlooping (looping) floats are found in the range associated with the loopers (nonloopers) regime, indicating that transition events may have taken place from one regime to the other.

The distribution of instantaneous spin predicted by two-dimensional LSMs was studied in Reynolds and Veneziani (2004), and an initial comparison with results obtained from MICOM floats longer than 60 days was carried out. The purpose was mainly to investigate the theoretical form of the spin distribution, confirming the results by means of the independently determined MICOM spin statistics. Here, we perform a number of LSM simulations with slightly modified conditions with respect to model (1), in order to achieve two goals. First, we intend to investigate the effects of a more complex than tri-modal Ω distribution on the eddy statistics. Second, we aim at verifying the result of taking into account transitions between loopers and nonloopers regimes.

Four LSM simulations have been carried out and the eddy statistics estimated from the simulated trajectories have been compared. The first simulation (LSM0) is the one performed in the first part of this paper, and it is characterized by a tri-modal distribution of Ω. The second simulation (LSM1) has the cyclonic mean spin uniformly distributed around a mean value which corresponds to the fixed Ω value used in LSM0, and with a variance $\sigma_\Omega = 0.1$ days^{-1}. The third simulation (LSM2) has the same Ω-pdf as LSM0, but it incorporates transitions from nonloopers to loopers regimes and vice versa. The probability, $P_{n\to l}$, for a nonlooper to become a looper during a period of 110 days (float's life) is taken equal to 9% (estimated from 60-day running-averaged Ω values computed from the MICOM trajectories). The corresponding probability, $P_{l\to n}$, for the opposite transition is calculated as n/l $\cdot$ $P_{n\to l}$, in order to maintain the relative populations of nonloopers ($n = 73.8\%$) and loopers ($l = 26.2\%$). This simulation is aimed at taking into account the nonstationarity events that occur when coherent vortices evolve in time, thus producing dramatic changes into the motion characteristics of the particles embedded inside the vortices. The last simulation (LSM3) considers both the effects of a flat Ω-pdf and the effects of transitions. The basic parameters used in all four simulations are the ones displayed in the above Table 1.

The results of the LSM simulations in terms of Ω-frequency distribution (computed from the overall trajectory data set) are presented in Figure 7. The corresponding histogram plot obtained from the MICOM trajectories (Fig. 6a) is superposed, in order to facilitate the comparison.

The simulation LSM0 (Fig. 7a) provides mean spin values distributed mainly around the three averaged Ω_0 values used to characterize the nonloopers, the cyclonic, and the

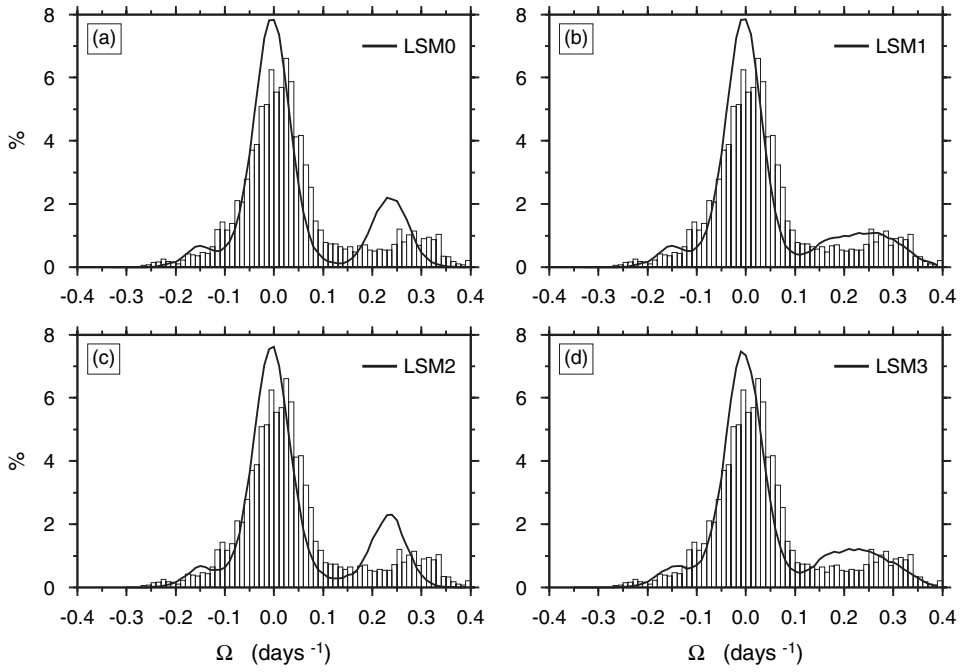

Figure 7. Frequency distributions of Ω values estimated from the overall MICOM Lagrangian data set in RINGS (histogram), and from the trajectories simulated in (a) LSM0, (b) LSM1, (c) LSM2, and (d) LSM3 (solid lines).

anticyclonic trajectories. The frequency distribution is able to capture the main features of the Ω-histogram obtained from the MICOM floats, which are the concentration of mean spin values around the nonloopers $\Omega = 0$, and the representation of the two secondary peaks corresponding to the loopers averaged Ω values. The results, however, cannot describe the details of the distribution of the higher spin parameters and the intermediate values of Ω found between the nonloopers and loopers regimes.

Better agreement is attained with the simulation LSM1 (Fig. 7b), reflecting the fact that a number of different values of Ω characterized by a uniform probability distribution have been attributed to the cyclonic trajectories. This property of the Ω-pdf has also the effect of slightly improving the description of the velocity autocovariance function for the cyclones and the overall trajectories, as it can be seen in Figure 8. The plot, which compares the MICOM zonal autocovariance (thick line) with the LSM0 and LSM1 corresponding statistics (thin and dash-dotted line, respectively), shows that the oscillating pattern of the LSM1 autocovariance follows the MICOM statistics more closely than the LSM0 results. The LSM1 statistics exhibits a less pronounced amplitude of the oscillations, compatible with the argument that the different contribution of a number of structures characterized by different scales tend to dampen down the oscillations of the dominant signal. Simulation

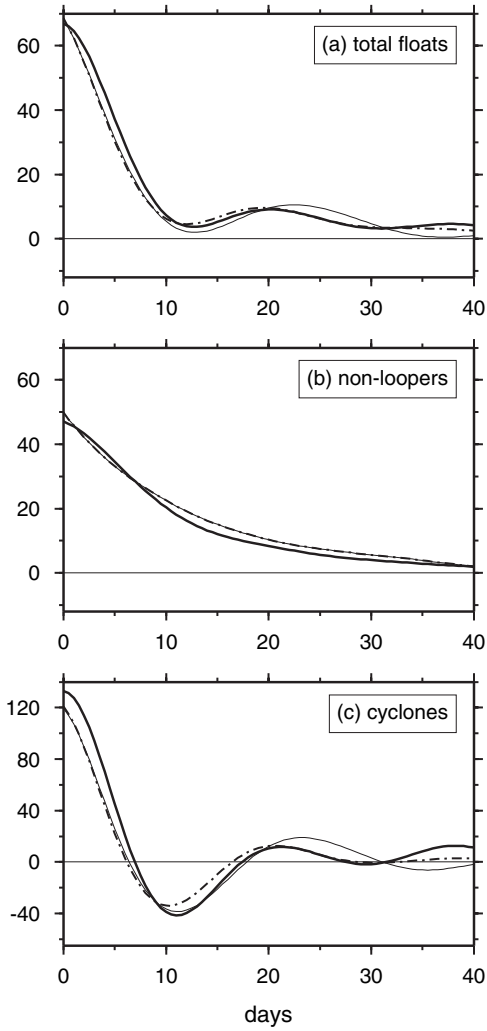

Figure 8. Comparison between the zonal velocity autocovariance functions computed from the MICOM floats (thick line), the LSM0 (thin line), and the LSM1 trajectories (dash-dotted line), for the three different data subsets.

LSM1, however, produces no appreciable changes in the predicted eddy dispersion function D (not shown), thus suggesting that the dominant coherent vortex structures have the highest influence on the particle dispersion properties.

The simulation LSM2 (Fig. 7c) shows a slight improvement in predicting the MICOM Ω-histogram plot for mean spin values ranging between the nonlooper and the cyclonic regimes. The difference with the LSM0 results, however, is minimal, also in terms of autocovariance and eddy dispersion. This may be partially due to the fact that the transition

probability $P_{n\to l} = 9\%$ does not reflect completely the real transition events taking place between nonloopers and loopers regimes. A more precise assessment of the actual transition time scale and probability distribution needs to be carried out.

Finally, simulation LSM3 (Fig. 7d) gives a superposition of results from LSM1 and LSM2. The predicted autocovariance statistics are very similar to the ones obtained from the LSM1 simulated trajectories, suggesting that the effects of the flat Ω distribution tend to dominate those induced by regime transitions. The overall eddy dispersion function is also basically unchanged with respect to simulation LSM0.

The conclusion we draw from such LSM simulations is that, although a more complex distribution of Ω seems appropriate, the main characteristics of the autocovariance functions and other statistics, in terms of oscillation patterns and time scales, are only slightly changed. This is likely due to the fact that the RINGS region is energetically dominated by coherent vortices (Gulf Stream cold-core rings) characterized by similar temporal and spatial scales. Different and more significant effects of a flat Ω-pdf may be expected in other oceanic regions or at different depth levels. The results of this section justify the bi-modality (or tri-modality) hypothesis utilized in the present work and in the previous V04, V05.

6. Summary and conclusions

In this paper, we have used 700 m MICOM Lagrangian data for the southern Gulf Stream recirculation region to investigate the properties of eddy diffusivity and single-particle dispersion in the presence of coherent vortices, and to test the applicability of a Lagrangian stochastic model to parameterize these characteristics. We have also studied the frequency distribution of the Ω parameter that is used to represent the looping behavior of trajectories embedded inside energetic coherent vortices.

The main conclusion is that the LSM with spin is successful in reproducing the eddy diffusivity and the particle dispersion characteristics, particularly at short and intermediate time scales. The effects of the coherent vortices are correctly taken into account, in terms of enhanced spreading of particles at short times due to the high energy content of the vortices, and reduced spreading at longer times due to the trapping mechanisms of the vortex coherent structure. The results can be directly used in Lagrangian oceanographic applications in which the eddy transport of tracers need to be parameterized. Previous investigators have used either observed large-scale velocity fields or numerical velocity outputs simulated by low-resolution OGCMs, in conjunction with first-order, one-dimensional (without spin) LSMs to describe the turbulent spreading of ocean pollutants, biological quantities, or water particles in regions not dominated by coherent structures (e.g., Aamo *et al.,* 1997; Cetina *et al.,* 2000; Cowen *et al.,* 2000, 2003; Falco *et al.,* 2000; Paris *et al.,* 2002). The introduction of the two-dimensional spin model is expected to provide a very useful tool for regions with strong instabilities, where significant coherent structures and vortices are generated. A further development that could be particularly useful for climatic applications is the Lagrangian stochastic modeling of the coherent

vortex drift, which was subtracted from the total loopers velocities in the present paper. The drift could be part of the subgrid scale flow not completely resolved by low-resolution, climate OGCMs and should also be parameterized. Another practical application of the spin LSM would be to evaluate estimates of eddy fluxes, such as eddy heat transport, more appropriately than in the typically used eddy-diffusivity parameterization.

The comparison of the eddy dispersion predicted by the LSM with the results obtained by applying the asymptotic eddy-diffusivity approximation shows that the eddy-diffusivity theory tends to overestimate the actual dispersion processes. This is because the estimate of the eddy diffusivity parameter K is asymptotic and is strictly related to the eddy kinetic energy level and to the very difficult quantity to estimate that is either the time or the space scale associated with the eddy field. Larger discrepancies are found at short and intermediate time scales and in the cases in which K is computed through Eulerian rather than Lagrangian data.

The issue of estimating as appropriate as possible values of K assumes importance when considering that the eddy-diffusivity parameterization (although valid under conditions that do not always occur in reality) is commonly employed in OCGMs to describe the eddy contribution to the spreading of passive and quasi-passive tracers. We acknowledge that reliable asymptotic values of diffusivity such as the ones estimated here from the extensive MICOM Lagrangian data set, are generally hard to obtain from *in-situ* floats due to the typical insufficient data coverage available at long times. We nevertheless suggest consideration of an "inverse" application of the Lagrangian stochastic model with spin, through which K can be estimated without the computation of asymptotic parameters by using the LSM theoretical expression of eddy diffusivity. This methodology, which has already been adopted in past investigations (Griffa *et al.,* 1995; Griffa, 1996; Berloff and McWilliams, 2002), was applied in RINGS and provided averaged estimates of K that were comparable with those directly computed from the MICOM Lagrangian diffusivities. It could therefore be used to provide K estimates for low-resolution OGCMs, more appropriate than those obtained from Eulerian data.

Another conclusion of this paper concerns the investigation of the mean spin probability distribution. The Ω frequency histogram was found to be more complex than the simple tri-modal distribution considered in V04 and in the benchmark LSM simulation of the present work. This could be due either to the presence of coherent vortices characterized by different spatial and temporal scales or, as thoroughly discussed in V05, to the time evolution of the vortices which exhibits weakening and strengthening events mostly because of ring-stream and ring-ring interactions. The inclusion of a complex Ω-pdf in the first-order, two-dimensional LSM (1) has, nonetheless, produced only slight changes in the covariance and dispersion functions, most probably because of the energetic dominance of a particular coherent vortex structure (Gulf Stream rings) in the investigated region. More substantial effects may be possible over other geographical areas or at different depth levels.

The existence of two separated regimes associated with the coherent vortices and the

background eddy field, and the fact that their superposition determines the overall characteristics of the turbulent flow, resemble quite closely the results of two-dimensional and quasi-geostrophic turbulence theory (Elhmaidi *et al.,* 1993; Provenzale, 1999; Bracco *et al.,* 2000). Most of these studies, however, concentrate on the nonlocal effects of coherent vortices on the background turbulent field. The energetic vortex structures tend to disturb the background flow by introducing nongaussianities in the velocity pdf (i.e., intermittent but very energetic events in an otherwise quiet environment) and anomalous diffusion properties (Elhmaidi *et al.,* 1993; Bracco *et al.,* 2000; Reynolds, 2002). Furthermore, Pasquero *et al.* (2001) show that the background eddy field is characterized by two distinct decorrelation time scales, one intrinsically associated with the background flow and one, much shorter, due to the nonlocal effects of the coherent vortices. For this reason, they find that even the background eddy field is not simply described by a linear stochastic process of the first order. In this paper, we have not considered the effects of the vortices on the background flow (although the nonloopers autocovariance function in Figure 1b seem to show two different decaying time scales before and after $\tau \approx 12$ days). We believe, in fact, that this phenomenon is difficult to isolate and properly quantify, due to the existence of a number of dynamical features and coherent structures possibly influencing the oceanic eddy field.

Acknowledgments. The authors wish to thank Bill Johns and Arthur Mariano for suggestions and helpful scientific discussions. The research was supported by the National Science Foundation through grant OCE-9811358. A. Griffa also acknowledges the support of the Office of Naval Research through grant N00014-97-1-0620. A. Reynolds was partially supported by the BBSRC through a core strategic grant.

APPENDIX

Investigation of anisotropy in the eddy statistics

Possible reasons for the anisotropic features of the eddy statistics in the RINGS region are investigated in the following. The problem will be addressed focusing on the nonloopers statistics, whose anisotropy is particularly evident (Fig. 1b). The slight anisotropy of the loopers autocovariances (Fig. 1c) is most probably influenced by the lower sampling of the loopers data set and by the incomplete estimate of the loopers translation speed subtracted from the total Lagrangian velocities (see V05 for details). In order to facilitate the discussion, a brief description of the method used to estimate velocity autocovariance functions and single-particle dispersion from trajectory data is first provided.

The Lagrangian statistics are estimated as ensemble averages over the statistics computed from a sufficiently high number of trajectories. In the case of velocity autocovariance function (similar estimates are carried out for the crosscovariances), the averaged R is obtained by ensemble averaging the single trajectory autocovariances, $R^{(p)}$, at each time lag $\tau = (k - 1)\Delta t$,

$$R^{(p)}(\tau) = \frac{1}{N^{(p)} - k + 1} \sum_{i=1}^{N^{(p)}-k+1} u_i^{(p)} u_{i+k-1}^{(p)}, \tag{A1}$$

$$R(\tau) = \frac{\sum_{p=1}^{part} (N^{(p)} - k + 1) R^{(p)}(\tau)}{\sum_{p=1}^{part} (N^{(p)} - k + 1)}, \tag{A2}$$

where $N^{(p)}$ is the total number of data available for the p trajectory, $k = 1, 2, \ldots, N^{(p)}$, and $part$ is the total number of trajectories. The velocities refer to the eddy fluctuation field u', but the primes have been dropped to ease the notation.

The averaging method (A1), which implicitly assumes stationarity and homogeneity, is applied in order to reduce the dependency of the instantaneous value of $u_i^{(p)} u_{i+k-1}^{(p)}$ on the particular state of the eddy velocity at $t_i = (i - 1)\Delta t$, while preserving the fundamental dependency of $R^{(p)}$ on the time lag τ. The ensemble average (A2) at each time lag is computed by weighing the single trajectory autocovariance, $R^{(p)}$, by the number of data available for that particular trajectory at that particular time lag. This implies that longer trajectory records contribute more to the final estimate of R.

Analogous methods of computing the eddy dispersion functions are applied,

$$D^{(p)}(\tau) = \frac{1}{N^{(p)} - k + 1} \sum_{i=1}^{N^{(p)}-k+1} (x_{i+k-1}^{(p)} - x_i^{(p)})^2, \tag{A3}$$

$$D(\tau) = \frac{\sum_{p=1}^{part} (N^{(p)} - k + 1) D^{(p)}(\tau)}{\sum_{p=1}^{part} (N^{(p)} - k + 1)}, \tag{A4}$$

where $x^{(p)}$ is the eddy displacement determined by integrating the eddy velocity $u^{(p)}$ along the p trajectory, with respect to an arbitrary initial position x_0 common to all floats. In this paper, the ensemble averages (A2) and (A4) have been computed for the entire Lagrangian data set and for the separate subsets of the loopers and nonloopers.

A possible reason for the anisotropy shown in Figure 1 is that the Lagrangian statistics are influenced by trajectory sampling due to the rectangular shape of the RINGS region. Long trajectories living in RINGS ought to be mostly zonal because large meridional excursions would drive them out of the region. At long time lags, these zonal floats may contribute with their lower meridional velocities to underestimate the eddy statistics in the meridional direction. In order to investigate this sampling effect, the autocovariance R has been estimated by varying the length of the trajectories taken into account in the averaging process (A1). In particular, instead of using $N^{(p)}$ (i.e., the whole trajectory record) only the first N_{cut} points are considered for each float, corresponding to the temporal record $T_{cut} = (N_{cut} - 1)\Delta t$, and the changes of R at varying T_{cut} are investigated. Floats with life shorter than T_{cut} are also included in the averaging process, and their $R^{(p)}$ is again estimated over their whole trajectory record $N^{(p)}$ (because, in these cases, $N^{(p)} \leq N_{cut}$). For short T_{cut} values, when virtually all floats are still inside RINGS, the average (A2) depends on all the trajectories with approximately equal weight, and it is therefore representative of the whole

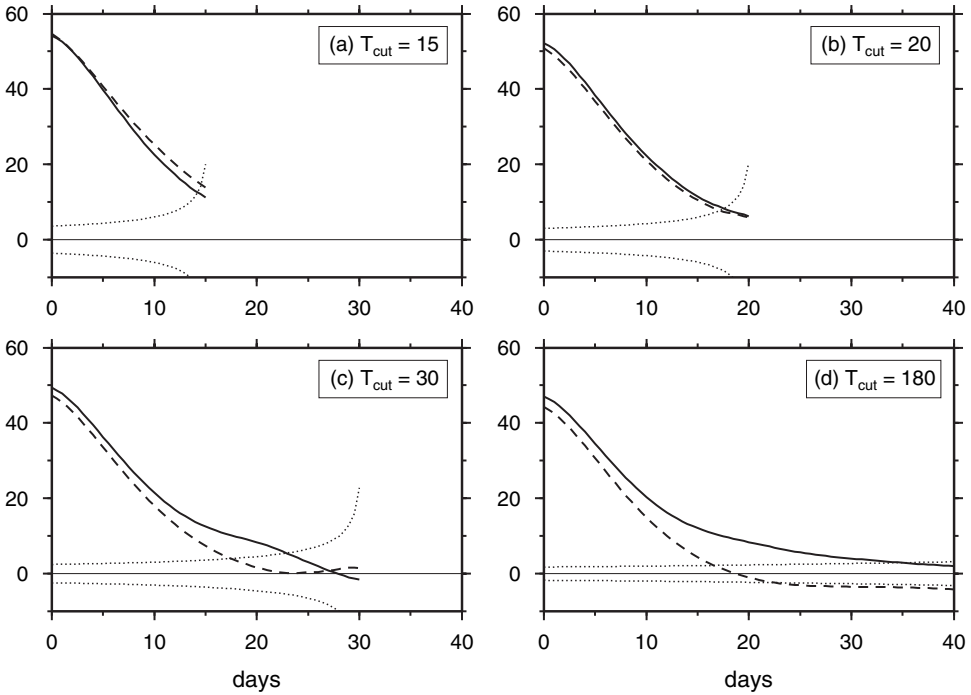

Figure A1. Nonloopers velocity autocovariance functions obtained by changing the number of points along the trajectories used for the statistical estimate (A1). Instead of using the whole trajectory record to estimate R, only the first N_{cut} points are considered for each float, corresponding to $T_{cut} = (N_{cut} - 1)\Delta t$. Values of T_{cut} are given in days.

ensemble available in RINGS. When T_{cut} is increased, longer trajectories tend to dominate the statistics (A2) even at short time lags because of the average process (A1). As a consequence, if the short-lag statistics vary significantly at increasing T_{cut}, this is an indication of the presence of a "bias" induced by the long-lived floats. Results of nonloopers autocovariance functions obtained with $T_{cut} = 15$, 20, 30, and 180 days are shown in Figure A1 (note that, since the maximum length of MICOM floats is 6 months, the case $T_{cut} = 180$ corresponds to considering the whole floats record as in Fig. 1b).

The statistics show a significant difference of pattern at varying T_{cut}. When $T_{cut} = 15$ and 20 days (Fig. A1a, b), the autocovariances are basically isotropic exhibiting a slightly higher energy than that shown from the autocovariance functions of the whole nonloopers data set (Fig. A1d). At $T_{cut} = 30$ days the anisotropy is evident, even at short time lags ($\tau \leq 10$ days), suggesting the presence of a bias due to the longer trajectories. The zonal autocovariance exhibits a "knee" feature around $\tau = 20$ days, and the meridional autocovariance starts showing a suppressed level of diffusion. At longer time scales, the statistics remain essentially unchanged and similar to the pattern observed when considering the whole trajectory records (Fig. A1d).

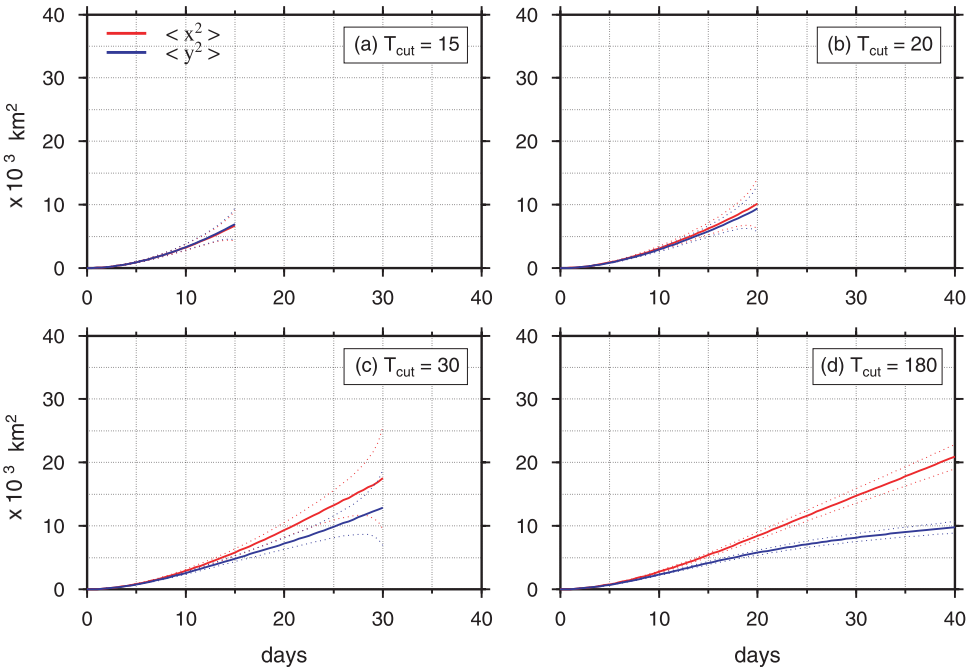

Figure A2. Nonloopers dispersion functions computed in a similar fashion as for the statistics in Figure A1.

A similar behavior is seen when considering the nonloopers dispersion statistics D at varying T_{cut} values, shown in Figure A2. At $T_{cut} = 15$ and 20 days (Fig. A2a, b), dispersions are highly isotropic, whereas from $T_{cut} = 30$ days the effect of the longer trajectories is to suppress particle dispersion in the meridional direction starting from time lag $\tau = 10$ days. The dispersion function in Figure A2b also shows that, on average, float displacement reaches ≈100 km at time scales of 20 days. Since the RINGS meridional extension varies between 1° and 1.5° with respect to a central zonal axis, the dispersion characteristics suggest that after 20 days particles are close to the meridional border and tend to leave the RINGS region through it. The anisotropy seen at long T_{cut} values could then be partially due to the earlier departure of fast moving trajectories from RINGS.

Conceptually, we expect that the statistics obtained for small T_{cut} values (15–20 days) are more representative of the whole particle ensemble, especially at short scales. The variance σ^2 and the time scale T_L of the process appear, therefore, approximately isotropic, at least at short-intermediate time lags. This is the reason for the isotropic parameters chosen in the LSM simulations of the paper (Table 1, estimates performed from the statistics at $T_{cut} = 20$ days).

Finally, the existence of a sampling effect is also indirectly indicated by the behavior of the eddy statistics computed in Section 3 from the LSM-simulated particles falling inside a

region resembling the shape of RINGS. Although no anisotropy is introduced in the LS model both in terms of parameters and physics, the meridional autocovariance function of the LSM trajectories (Fig. 1e) shows a negative lobe at time scales comparable with those observed in the MICOM statistics (Fig. 1b).

Despite evidence of Lagrangian sampling, we believe that there is also a more fundamental physical process responsible for the observed statistical anisotropy. Previous studies of both numerical and in-situ float trajectories (e.g., Freeland *et al.,* 1975; LaCasce and Speer, 1999; LaCasce, 2000; O'Dwyer *et al.,* 2000) have, in fact, suggested that floats spread preferentially along contours of potential vorticity. Furthermore, the inhomogeneity characteristics of the Gulf Stream recirculation region can be the cause of preferential dispersion in the zonal rather than in the meridional direction. North of the RINGS region, the Gulf Stream jet acts as a physical barrier to meridional spreading of particles, while south of RINGS both the large-scale mean flow and the eddy kinetic energy field exhibit very low values, thus inducing low levels of meridional as well as zonal particle spreading. Identifying and quantifying the specific physical mechanisms and separating their effect from the Lagrangian sampling effect, proved to be a difficult task because of the dynamically complex features of the Gulf Stream recirculation area. Further process studies are needed to address properly this point, and to quantify the relative importance of Lagrangian sampling over more fundamental processes responsible for the observed anisotropy.

REFERENCES

Aamo, O. M., M. Reed and K. Dowing. 1997. Oil spill contingency and response (OSCAR) model system: sensitivity studies, *in* Proceeding of the 1997 International Oil Spill Conference, Fort Lauderdale, USA, April 7–10, 1997.

Bauer, S., M. S. Swenson and A. Griffa. 2002. Eddy-mean flow decomposition and eddy-diffusivity estimates in the tropical Pacific Ocean. 2. Results. J. Geophys. Res., *107,* 3154, doi:10.1029/2001JC000613.

Bauer, S., M. S. Swenson, A. Griffa, A. J. Mariano and K. Owens. 1998. Eddy-mean flow decomposition and eddy-diffusivity estimates in the tropical Pacific Ocean. 1. Methodology. J. Geophys. Res., *103,* 30855–30871.

Berloff, P. S. and J. C. McWilliams. 2002. Material transport in oceanic gyres. Part II: Hierarchy of stochastic models. J. Phys. Oceanogr., *32,* 797–830.

Berloff, P. S., J. C. McWilliams and A. Bracco. 2002. Material transport in oceanic gyres. Part I: Phenomenology. J. Phys. Oceanogr., *32,* 764–796.

Boning, C. W. and M. D. Cox. 1988. Particle dispersion and mixing of conservative properties in an eddy-resolving model. J. Phys. Oceanogr., *18,* 320–338.

Borgas, M. S., T. K. Flesch and B. L. Sawford. 1997. Turbulent dispersion with broken reflectional symmetry. J. Fluid Mech., *279,* 69–99.

Bracco, A., J. H. LaCasce, C. Pasquero and A. Provenzale. 2000. The velocity distribution of barotropic turbulence. Phys. Fluids, *12,* 2478–2488.

Cetina, M., R. Rajar and P. Provinec. 2000. Modelling of circulation and dispersion of radioactive pollutants in the Japan Sea. Oceanol. Acta, *23,* 819–836.

Cowen, R. K., K. M. M. Lwiza, S. Sponaugle, C. B. Paris and D. B. Olson. 2000. Connectivity of marine populations: Open or closed? Science, *287,* 857–859.

Cowen, R. K., C. B. Paris, D. B. Olson and J. L. Fortuna. 2003. The role of long distance dispersal versus local retention in replenishing marine populations. Gulf Carib. Res., *14,* 129–137.

Csanady, G. T. 1980. Turbulent Diffusion in the Environment, Dordrecht, D. Reidel Publ. Co., 248 pp.

Elhmaidi, D., A. Provenzale and A. Babiano. 1993. Elementary topology of two-dimensional turbulence from a Lagrangian view-point and single particle dispersion. J. Fluid Mech., *257,* 533–558.

Falco, P., A. Griffa, P.-M. Poulain and E. Zambianchi. 2000. Transport properties in the Adriatic Sea as deduced from drifter data. J. Phys. Oceanogr., *30,* 2055–2071.

Figueroa, H. A. and D. B. Olson. 1994. Eddy resolution versus eddy diffusion in a double gyre GCM. Part I: The Lagrangian and Eulerian description. J. Phys. Oceanogr., *24,* 371–386.

Freeland, H., P. Rhines and H. T. Rossby. 1975. Statistical observations of the trajectories of neutrally buoyant floats in the North Atlantic. J. Mar. Res., *33,* 383–404.

Griffa, A. 1996. Applications of stochastic particle models to oceanographic problems, *in* Stochastic Modeling in Physical Oceanography, P. M. R. Adler and B. Rozovskii, eds., Birkhäuser Verlag, 114–140.

Griffa, A., K. Owens, L. Piterbarg and B. Rozovskii. 1995. Estimates of turbulence parameters from Lagrangian data using a stochastic particle model. J. Mar. Res., *53,* 371–401.

Held, I. and V. D. Larichev. 1996. A scaling theory for horizontally homogeneous, baroclinically unstable flow on a beta-plane. J. Atmos. Sci., *53,* 946–952.

Krauss, W. and C. W. Boning. 1987. Lagrangian properties of the eddy fields in the northern Atlantic as deduced from satellite-tracked buoys. J. Mar. Res., *45,* 259–291.

LaCasce, J. H. 2000. Floats and *f*/*H*. J. Mar. Res., *58,* 61–95.

LaCasce, J. H. and K. G. Speer. 1999. Lagrangian statistics in unforced barotropic flows. J. Mar. Res., *57,* 245–274.

Lumpkin, R. and P. Flament. 2001. Lagrangian statistics in the central North Pacific. J. Mar. Syst., *29,* 141–155.

Lumpkin, R., A.-M. Treguier and K. Speer. 2002. Lagrangian eddy scales in the northern Atlantic Ocean. J. Phys. Oceanogr., *32,* 2425–2440.

O'Dwyer, J., R. G. Williams, J. H. LaCasce and K. G. Speer. 2000. Does the potential vorticity distribution constrain the spreading of floats in the North Atlantic. J. Phys. Oceanogr., *30,* 721–732.

Owens, W. B. 1991. A statistical description of the mean circulation and eddy variability in the northwestern Atlantic using SOFAR floats. Prog. Oceanogr., *28,* 257–303.

Paris, C. B., R. K. Cowen, K. M. M. Lwiza, D.-P. Wang and D. B. Olson. 2002. Multivariate objective analysis of the coastal circulation of Barbados, West Indies: implication for larval transport. Deep-Sea Res., *49,* 1363–1386.

Pasquero, C., A. Provenzale and A. Babiano. 2001. Parameterization of dispersion in two-dimensional turbulence. J. Fluid Mech., *439,* 279–303.

Poulain, P.-M. and P. P. Niiler. 1989. Statistical analysis of the surface circulation in the California Current System using satellite-tracked drifters. J. Phys. Oceanogr., *19,* 1588–1603.

Priestley, M. B. 1981. Spectral Analysis and Time Series, Academic Press. 890 pp.

Provenzale, A. 1999. Transport by coherent barotropic vortices. Ann. Rev. Fluid Mech., *31,* 55–93.

Reynolds, A. M. 2002. Lagrangian stochastic modeling of anomalous diffusion in two-dimensional turbulence. Phys. Fluids, *14,* 1442–1449.

—— 2003. Third-order Lagrangian stochastic modeling. Phys. Fluids, *15,* 2773–2777.

Reynolds, A. M. and M. Veneziani. 2004. Rotational dynamics of turbulence and Tsallis statistics. Phys. Lett. A, *327,* 10–15.

Richardson, P. L. 1993. A census of eddies observed in North Atlantic SOFAR float data. Prog. Oceanogr., *31,* 1–50.

Rupolo, V., V. Artale, B. L. Hua and A. Provenzale. 1996. Lagrangian velocity spectra at 700 m in the western North Atlantic. J. Phys. Oceanogr., *26,* 1591–1607.

Sawford, B. L. 1999. Rotation of trajectories in Lagrangian stochastic models of turbulent dispersion. Bound.-Layer Meteor., *93,* 411–424.

Sciremammano, F. Jr. 1979. A suggestion for the presentation of correlations and their significance levels. J. Phys. Oceanogr., *9,* 1273–1276.

Stammer, D. 1997. Global characteristics of ocean variability estimated from regional TOPEX/POSEIDON altimeter measurements. J. Phys. Oceanogr., *27,* 1743–1769.

—— 1998. On eddy characteristics, eddy transports, and mean flow properties. J. Phys. Oceanogr., *28,* 727–739.

Taylor, G. I. 1921. Diffusion by continuous movements. Proc. Lond. Math. Soc., *20,* 196–212.

Tennekes, H. and J. L. Lumley. 1972. A First Course in Turbulence, MIT Press. 300 pp.

Thomson, D. J. 1986. A random walk model of dispersion in turbulent flows and its application to dispersion in a valley. Quart. J. R. Met. Soc., *112,* 511–530.

Veneziani, M., A. Griffa, Z. D. Garraffo and E. P. Chassignet. 2005. Lagrangian spin parameter and coherent structures from trajectories released in a high-resolution ocean model. J. Mar. Res., *63,* 753–788.

Veneziani, M., A. Griffa, A. M. Reynolds and A. J. Mariano. 2004. Oceanic turbulence and stochastic models from subsurface Lagrangian data for the Northwest Atlantic Ocean. J. Phys. Oceanogr., *34,* 1884–1906.

Received: *1 April, 2005;* revised: *5 July, 2005.*